Schrödingerization for quantum linear systems problems

Yin Yang* Yue Yu[†] and Long Zhang[‡]

Hunan Key Laboratory for Computation and Simulation in Science and Engineering, Key Laboratory of Intelligent Computing and Information Processing of Ministry of Education, National Center for Applied Mathematics in Hunan, School of Mathematics and Computational Science, Xiangtan University, Xiangtan, Hunan 411105, China

Abstract

We develop a quantum algorithm for linear algebraic equations Ax = b from the perspective of Schrödingerization-form problems, which are characterized by a system of linear convection equations in one higher dimension. When A is positive definite, the solution x can be interpreted as the steady-state solution to a system of linear ordinary differential equations (ODEs). This ODE system can be solved by using the linear combination of Hamiltonian simulation (LCHS) method in [1], which serves as the continuous implementation of the Fourier transform in the Schrödingerization method from [2,3]. Schrödingerization transforms linear partial differential equations (PDEs) and ODEs with non-unitary dynamics into Schrödinger-type systems via the so-called warped phase transformation that maps the equation into one higher dimension. Compared to the LCHS method, Schrödingerization may be more appealing to the PDE community, as it is better suited for leveraging established computational PDE techniques to develop quantum algorithms. When A is a general Hermitian matrix, the inverse matrix can still be represented in the LCHS form in [1], but with a kernel function based on the Fourier approach in [4]. Although this LCHS form provides the steady-state solution to a system of linear ODEs associated with the least-squares equation, applying Schrödingerization to this least-squares system is not appropriate, as it results in a much larger condition number. We demonstrate that in both cases, the solution x can be expressed as the LCHS of Schrödingerization-form problems, or equivalently, as the steady-state solution to a Schrödingerization-form problem. This highlights the potential of Schrödingerization in quantum scientific computation. We provide a detailed implementation and error analysis, along with several numerical tests that validate the correctness of our proposed method. Furthermore, we develop a quantum preconditioning algorithm that combines the well-known BPX multilevel preconditioner with our method to address the finite element discretization of the Poisson equation.

Keywords: Linear systems problem, Schrödingerization, LCHS, preconditioning, Quantum algorithms.

MSCcodes: 68Q25, 68R10, 68U05.

^{*}yangyinxtu@xtu.edu.cn

 $^{^{\}dagger}$ terenceyuyue@xtu.edu.cn

 $^{^{\}ddagger}$ longzhang@smail.xtu.edu.cn

1 Introduction

Quantum computing is an emerging computational paradigm that has attracted significant attention, primarily due to the discovery of quantum algorithms capable of offering exponential speedups over the best-known classical methods [5–9]. Numerous quantum algorithms for scientific computing have been proposed in recent years. One fundamental task that underlies many areas of science and technology is the development of solvers for a linear system of equations

$$Ax = b, (1.1)$$

where A is an $N \times N$ invertible matrix with $N = 2^n$. In the realm of quantum computing, these are known as quantum linear systems algorithms (QLSAs), with the HHL algorithm [4,9,10] being a prominent example.

Classical solvers for linear systems typically take time proportional to the number of unknown variables, making them computationally expensive for large systems. This is especially true for systems arising from the numerical discretization of high-dimensional partial differential equations (PDEs). The HHL algorithm, introduced by Harrow, Hassidim, and Lloyd in 2009 [9], is the first quantum algorithm proposed for solving linear systems. Its gate complexity is $\mathcal{O}(\log(N)s^2\kappa^2/\delta)$, where κ is the condition number of the matrix, s is the sparsity of A, and δ is the precision. In contrast, for positive-definite matrices, the Conjugate Gradient (CG) method has a time complexity of $\mathcal{O}(Ns\sqrt{\kappa}\log(1/\delta))$, which exhibits polynomial growth with respect to N, making the HHL algorithm exponentially faster for large systems when the condition number κ of the matrix is not excessively large. To address the limitations of phase estimation in the HHL algorithm, Ambainis [11] introduced the variable-time amplitude amplification (VTAA) method, which improves the dependence on the condition number, reducing it from κ^2 to $\kappa \log^3(\kappa)$. Building on this, Childs et al. [4] further improved the algorithm, achieving a nearly linear dependence on the condition number. To enhance the accuracy dependence, they replaced the Hamiltonian simulation with either the Fourier method or the Chebyshev method, resulting in a polylog $(1/\delta)$ dependence. This is similar to the dependence observed in classical methods and provides an exponential acceleration in accuracy compared to the HHL algorithm. However, the VTAA procedure is highly complex, involving multiple rounds of recursive amplitude amplification, which makes it difficult to implement in practice [10]. To address this issue, alternative approaches based on adiabatic quantum computing (AQC) have been developed in recent years. Dong et al. [12] proved that by employing an optimally tuned scheduling function, AQC is capable of efficiently solving a quantum linear system problem (QLSP) with a runtime of $\mathcal{O}(\kappa \text{poly} \log(\kappa/\delta))$. Lin et al. [13] proposed a quantum eigenstate filtering algorithm and introduced Zeno eigenstate filtering when applying it to the QLSP. One can also refer to [10] for a comprehensive review of the literature along this line, where the optimal scaling with the condition number is achieved with query complexity $\mathcal{O}(\kappa \log(1/\delta))$ by using a discrete quantum adiabatic theorem proved in [14], which completely avoids the heavy mechanisms of VTAA or the truncated Dyson-series subroutine from previous methods related to the AQC [15].

In this article, we aim at developing quantum algorithms for solving linear algebraic equations

from the perspective of Schrödingerization-form problems, which are characterized by a system of linear convection equations in one higher dimension. This approach is straightforward when A is positive definite. In this case, we can consider the solution x as the steady-state solution to the system of linear ordinary differential equations (ODEs) $u_t = -Au + b$, as described in [16]. The resulting linear ODE system is then solved by the Schrödingerization method introduced in [2,3]. Schrödingerization transforms linear PDEs and ODEs with non-unitary dynamics into Schrödinger-type systems via the so-called warped phase transformation that maps the equation into one higher dimension. The ODE system can also be resolved by using the linear combination of Hamiltonian simulation (LCHS) method in [1], which can be viewed as the continuous implementation of the Fourier transform in the Schrödingerization method. Compared to the LCHS method, Schrödingerization may be more attractive to the PDE community and more convenient to the use of the well-established computational PDE techniques to develop quantum algorithms. Another important feature of Schrödingerization is that, as a continuous-variable formulation, it is naturally suited for analog quantum computing, which could be realized in the nearer term compared with digital quantum computation [2,17].

For a general Hermitian matrix, it is unclear whether a Schrödingerization-based algorithm can be developed. However, it is evident that the inverse matrix A^{-1} can still be represented in the LCHS form from [1], but with a kernel function based on the Fourier approach in [4]. While this LCHS form provides the steady-state solution for a system of linear ODEs with coefficient matrix $-A^2$ and source term Ab, corresponding to the least-squares equations $A^2x = Ab$, applying Schrödingerization to this ODE system is not appropriate, as it results in a significantly larger condition number. Inspired by the similarities in the LCHS forms and recognizing that the LCHS method for linear ODEs can be recast as the Schrödingerization method, we successfully express the solution x as the LCHS of Schrödingerization-form problems. By applying the Duhamel's principle, we instead reformulate this integral form of the solution as the steady-state solution to a Schrödingerization-form problem. This highlights the potential of the Schrödingerization technique in quantum scientific computation. Based on this result, we are in a position to develop a quantum algorithm utilizing the discrete Fourier transform as done for the Schrödingerization method.

The time complexity of our algorithm still exhibits a quadratic dependence on the condition number. By employing the VTAA, as done in [4], we can reduce the κ -dependence from quadratic to nearly linear. However, the VTAA procedure is overly complex. On the other hand, for numerical solutions of PDEs, the condition number is often a dominant factor in determining the runtime. For instance, in the finite element discretization of the Poisson equation, the condition number grows as $\mathcal{O}(h^{-2})$, where h is the mesh size. As a result, the time complexity scales at least as $\mathcal{O}(h^{-2})$. This issue can be mitigated using preconditioning techniques in classical computation, which seek a matrix B such that $\kappa(BA) = \mathcal{O}(1)$, and then solve the modified linear system BAx = Bb. It is natural to extend this classical technique to the quantum scenario and combine it with our approach to develop highly efficient quantum algorithms for PDEs. We develop a quantum preconditioning algorithm that employs the well-known BPX multilevel preconditioner for the finite element discretization of the two-dimensional Poisson equation. The quantum realization of the

finite element method (FEM) with BPX preconditioning has been explored in [18], based on the symmetric form $S^{\dagger}ASy = S^{\dagger}b$, where y satisfies x = Sy and $\kappa(BA) = \kappa(S^{\dagger}AS)$. The block encoding of this symmetric preconditioned system in [18] is somewhat complex, and this has been improved in [19]. The algorithm in [19] uses the Schrödingerization approach, as A and B are positive definite, where the solution to the linear system is recast as the steady-state solution of the associated linear ODE system. However, as noted in [19], applying the Schrödingerization method to find the steady-state solution to the ODEs for the non-symmetric preconditioning system BAx = Bb becomes problematic when the evolution time is large, as the non-symmetry of BA introduces additional challenges in recovering the solution. In contrast, this issue does not arise in our algorithm, as it does not require recovering the solution over a range dependent of the evolution time for the auxiliary variable.

The paper is organized as follows. In Section 2, we introduce an abstract framework that expresses the inverse matrix as a linear combination of Hamiltonian simulations, characterized by kernel functions. We also formulate the corresponding evolution problems for two representative choices of kernel functions. Section 3 demonstrates how the LCHS formula can be transformed into an LCHS with a Hamiltonian defined by a system of linear convection equations in one higher dimension, which is referred to as a Schrödingerization-form problem in this work. In Section 4, we provide detailed implementation procedures along with an error analysis. Section 5 presents a series of numerical experiments that validate the accuracy and correctness of the proposed approach. The final section is dedicated to combining our algorithm with the multilevel preconditioning method for solving the finite element discretizations of the Poisson equation.

2 Linear combination of Hamiltonian simulation for the QLSP

In this section we introduce an abstract framework of solving the quantum linear system problem (QLSP), which represents the QLSP as a linear combination of Hamiltonian simulations e^{-iHt_i} , where $t_i \in \mathbb{R}$ and H is a Hermitian matrix defined by the coefficient matrix of the linear system.

Theorem 2.1. Let A be an invertible Hermitian matrix, and let $\eta(k)$ be a function defined on \mathbb{R} , with its Fourier transform given by

$$\hat{\eta}(s) = \int_{\mathbb{R}} \eta(k) e^{-iks} dk.$$

Assume that

$$\int_{0}^{\infty} \hat{\eta}(\lambda s) ds = \frac{1}{\lambda}, \qquad 0 \neq \lambda \in [\lambda_{\min}, \lambda_{\max}],$$

where λ_{\min} and λ_{\max} are the minimum and maximum eigenvalues of A, respectively. Then the inverse matrix A^{-1} can be represented as a linear combination of Hamiltonian simulation problems:

$$A^{-1} = \int_0^\infty \int_{\mathbb{R}} \eta(k) e^{-ikAs} dk ds.$$
 (2.1)

Proof. The result is obtained through the diagonalization of $A = U\Lambda U^{\dagger}$, where $\Lambda = (\lambda_1, \dots, \lambda_N)$ is a diagonal matrix and U is a unitary matrix.

Here we list two choices of the kernel function from the literature:

• Fourier approach in [4]:

$$\eta(k) = \varphi(k) := \frac{i}{\sqrt{2\pi}} k e^{-k^2/2}, \qquad \hat{\varphi}(s) = s e^{-s^2/2}.$$
(2.2)

• LCHS method for ODEs in [1,20] with A being positive definite:

$$\eta(k) = \psi(k) := \frac{f(k)}{1 - ik}, \qquad \hat{\psi}(s) = e^{-s} \quad (s \ge 0),$$

where $f(k) = \frac{1}{2\pi e^{-2\beta} e^{(1+ik)\beta}}$ is given in Eq. (32) of [1].

Remark 2.1. It should be noted that the first choice does not impose any requirements on the signs of the eigenvalues of A. One can also choose

$$\eta(k) = \rho(k) := \frac{1}{\pi} e^{-k^2/2}, \qquad \hat{\rho}(s) = \sqrt{\frac{2}{\pi}} e^{-s^2/2}.$$

Now we show that the LCHS for the QLSP can be reformulated as the steady-state solution to a system of ODEs.

Theorem 2.2. Let x denote the solution to (1.1), where A is an invertible Hermitian matrix. Additionally, for the LCHS method applied to ODEs, we assume that A is also positive definite. Then there holds $x = \lim_{t \to \infty} u(t)$, where u satisfies

$$\frac{\mathrm{d}\boldsymbol{u}}{\mathrm{d}t} = -A^k \boldsymbol{u} + A^{k-1} \boldsymbol{b}, \quad \boldsymbol{u}(0) = \boldsymbol{0}, \tag{2.3}$$

with k = 2 for the Fourier approach and k = 1 for the LCHS method for ODEs.

Proof. For the Fourier approach, we have

$$\int_0^t \hat{\varphi}(\lambda_j s) ds = \int_0^t \lambda_j s e^{-(\lambda_j s)^2/2} ds = \frac{1}{\lambda_j} \int_0^{\lambda_j t} s' e^{-s'^2/2} ds' = \frac{1}{\lambda_j} (1 - e^{-(\lambda_j t)^2/2}),$$

which implies

$$\int_0^t \int_{\mathbb{R}} \varphi(k) e^{-ikAs} dk ds = U^{\dagger} (I - e^{-(\Lambda t)^2/2}) \Lambda^{-1} U = (I - e^{-(At)^2/2}) A^{-1}.$$

For the LCHS method for ODEs, one can deduce the result in a similar manner.

The ODE system with k=2 is clearly stable when A is a Hermitian matrix, which contrasts with the ODE system with k=1.

3 Schrödingerization for quantum linear systems problems

In the following, we first demonstrate that the LCHS formula in Theorem 2.1 can be converted into the LCHS with the Hamiltonian given by convection equations in one higher dimension. This transformation allows us to apply the discrete Fourier transform, similar to the approach used in the Schrödingerization method for ODEs. This is straightforward when A is positive definite since we can consider the solution x as the steady-state solution to the ODE system in (2.3) with k = 1 as was done in [16]. For a general Hermitian matrix, applying Schrödingerization to (2.3) with k = 2 is not appropriate as it results in a significantly larger condition number.

Theorem 3.1. Let A be an invertible Hermitian matrix, and consider the linear system Ax = b. Then,

$$\boldsymbol{x} = A^{-1}\boldsymbol{b} = \int_0^\infty \boldsymbol{v}(t,0)dt,$$
(3.1)

where $\mathbf{v}(t,p)$ satisfies the following system of convection equations

$$\begin{cases} \frac{\mathrm{d}}{\mathrm{d}t} \boldsymbol{v}(t,p) = A \partial_p \boldsymbol{v}(t,p), \\ \boldsymbol{v}(0,p) = \zeta(p) \boldsymbol{b} \end{cases}$$
(3.2)

with $\zeta(p) = \hat{\varphi}(p) = p e^{-p^2/2}$. The above statement holds for $\zeta(p) = \hat{\psi}(p)$ if A is positive definite, where $\hat{\psi}(p) = e^{-p}$ for $p \ge 0$.

Proof. We first consider the Fourier approach,

$$A^{-1}\boldsymbol{b} = \int_0^\infty \int_{\mathbb{R}} e^{-ikAs} (\varphi(k)\boldsymbol{b}) dk ds.$$

Assume that $\boldsymbol{v}(t,p)$ is the Fourier transform of $\check{\boldsymbol{v}}(t,k) = \mathrm{e}^{-\mathrm{i}kAt}(\varphi(k)\boldsymbol{b})$, namely,

$$\boldsymbol{v}(t,p) = \int_{\mathbb{R}} \mathrm{e}^{-\mathrm{i}kp} \check{\boldsymbol{v}}(t,k) \mathrm{d}k = \int_{\mathbb{R}} \mathrm{e}^{-\mathrm{i}kp} \mathrm{e}^{-\mathrm{i}kAt} (\varphi(k)\boldsymbol{b}) \mathrm{d}k.$$

Noting that $\check{\boldsymbol{v}}(t,k)$ satisfies

$$\begin{cases} \frac{\mathrm{d}}{\mathrm{d}t} \check{\boldsymbol{v}}(t,k) = -\mathrm{i}kA\check{\boldsymbol{v}}(t,k), & \check{\boldsymbol{v}}(0,k) = \varphi(k)\boldsymbol{b}, \\ \lim_{|k| \to +\infty} \check{\boldsymbol{v}}(t,k) = \boldsymbol{0}, \end{cases}$$

we apply the Fourier transform to get

$$\begin{cases} \frac{\mathrm{d}}{\mathrm{d}t} \boldsymbol{v}(t,p) = A \partial_p \boldsymbol{v}(t,p), \\ \boldsymbol{v}(0,p) = \int_{\mathbb{R}} e^{-\mathrm{i}kp} \varphi(k) \mathrm{d}k \boldsymbol{b} = \hat{\varphi}(p) \boldsymbol{b} = p e^{-p^2/2} \boldsymbol{b}. \end{cases}$$

The solution x can be restored by

$$\boldsymbol{x} = A^{-1}\boldsymbol{b} = \int_0^\infty \boldsymbol{v}(t,0) dt.$$

For the LCHS method for ODEs, A is assumed to be positive definite. Following the above discussion, we obtain

$$\begin{cases} \frac{\mathrm{d}}{\mathrm{d}t} \boldsymbol{v}(t,p) = A \partial_p \boldsymbol{v}(t,p), \\ \boldsymbol{v}(0,p) = \int_{\mathbb{R}} e^{-\mathrm{i}kp} \psi(k) \mathrm{d}k \boldsymbol{b} = \hat{\psi}(p) \boldsymbol{b}. \end{cases}$$

By Eq. (36) in [1], $\hat{\psi}(p) = e^{-p}$ for $p \ge 0$.

Based on the above result, we can develop a quantum algorithm utilizing the discrete Fourier transform. Unlike the direct solution for an ODE problem, we need to address the integral with respect to the "artificial time" in (3.1).

To avoid the integration in (3.1), which involves a relatively complex LCU procedure, we reformulate (3.2) as an equivalent form with the initial data shifted into the source term. Here we only present the result for a general Hermitian matrix.

Corollary 3.1. Let A be an invertible Hermitian matrix, and consider the linear system $A\mathbf{x} = \mathbf{b}$. Then $\mathbf{x} = A^{-1}\mathbf{b} = \lim_{t \to \infty} \mathbf{v}(t, 0)$, where $\mathbf{v}(t, p)$ satisfies the following system of convection equations

$$\begin{cases} \frac{\mathrm{d}}{\mathrm{d}t} \boldsymbol{v}(t,p) = A \partial_p \boldsymbol{v}(t,p) + \zeta(p) \boldsymbol{b}, \\ \boldsymbol{v}(0,p) = \boldsymbol{0} \end{cases}$$
(3.3)

with
$$\zeta(p) = \hat{\varphi}(p) = pe^{-p^2/2}$$
.

Proof. The equivalence of Theorems 3.1 and 3.1 is precisely the Duhamel's principle, which simplifies the solution of non-homogeneous linear differential equations by expressing it as an integral that involves the homogeneous solution and the forcing function.

As previously noted, it is not appropriate to treat the solution to the linear system as the steady-state solution to a system of linear ODEs. Theorem 3.1 demonstrates that the solution can instead be interpreted as the steady-state solution to a system of linear convection equations in one higher dimension. In contrast to the standard Schrödingerization approach in [2,3], the convection system (3.3) can be viewed as a modified Schrödingerization of the ODE problem (2.3) (k = 1) with the auxiliary function $\zeta(p)$ replaced by the kernel function employed in the Fourier approach from [4]. However, this replacement makes the solutions between (3.3) and (2.3) not simply related since we no longer have the condition $\zeta'(p) = \pm \zeta(p)$ for $p \geq 0$. To avoid the LCU procedure, one possible approach is to first discretize the p-variable, which results in an ODE system, and then apply the standard Schrödingerization method. We do not explore this realization along this line in this article.

4 Implementation of the Schrödingerization form

In the context of the Schödingerization form, we focus solely on the kernel function for the Fourier method as it pertains to the general inversible Hermitian matrix. For a non-Hermitian matrix A, we introduce the dilation matrix $\tilde{A} = \begin{bmatrix} O & A \\ A^{\dagger} & O \end{bmatrix}$, which is Hermitian. Since \tilde{A} possesses both positive and negative eigenvalues, the kernel function for the Fourier method (or the one given in Remark 2.1) can only be applied in this case.

4.1 Discretization of the auxiliary variable

Let $p \in [a,b] = [-\pi R, \pi R]$ with R > 0 satisfying $\zeta(\pm \pi R) \approx 0$, where $\zeta(p)$ is defined in Theorem 3.1. Then one can apply the periodic boundary condition in the p direction and use the Fourier spectral method by discretizing the p domain. Toward this end, we choose a uniform mesh size $\Delta p = (b-a)/N_p$ for the auxiliary variable with $N_p = 2^{n_p}$ being an even number. The grid points are denoted by $a = p_0 < p_1 < \cdots < p_{N_p} = b$. For $p \in [a,b]$, the one-dimensional basis functions are usually chosen as

$$\phi_l(p) = e^{i\mu_l(p-a)}, \quad \mu_l = \frac{2\pi(l-N_p/2)}{b-a}, \quad l = 0, 1, \dots, N_p - 1.$$

We define the complex discrete Fourier space by

$$S_p = \text{span}\{\phi_l(p) : l = 0, 1, \dots, N_p - 1\}$$

and assume $u \in C_p[a, b]$, which is a continuous and periodic function on [a, b].

The Fourier interpolation $u_I \in S_p$ is defined by

$$u_I(p_k) = u(p_k), \quad k = 0, 1, \dots, N_p - 1.$$

Let

$$u_I(p) = \sum_{l=0}^{N_p - 1} \tilde{u}_l \phi_l(p). \tag{4.1}$$

The coefficients can be explicitly written as

$$\tilde{u}_l = \frac{1}{N_p} \sum_{k=0}^{N_p - 1} u(p_k) e^{-i\mu_l(p_k - a)}.$$

The interpolation can be written in matrix form as $u_I = u = \Phi \tilde{u}_l$, where

$$\mathbf{u}(t) = (u(p_j))_{N_p \times 1}, \quad \tilde{\mathbf{u}}_l = (\tilde{u}_l)_{N_p \times 1}, \quad \Phi = (\phi_{jl})_{N_p \times N_p} = (\phi_l(p_j))_{N_p \times N_p}.$$

The momentum operator $\hat{p}=-\mathrm{i}\partial_p$ can be discretized as

$$\hat{p}u(p) \approx \sum_{l=0}^{N_p-1} \tilde{u}_l(-\mathrm{i}\partial_p \phi_l(p)) = \sum_{l=0}^{N_p-1} \tilde{u}_l \mu_l \phi_l(p)$$

for $p = p_j$, $j = 0, 1, \dots, N_p - 1$, which is written in matrix form as

$$\hat{p}^{\mathbf{d}} \boldsymbol{u} = \Phi D_{\mu} \Phi^{-1} \boldsymbol{u} =: P_{\mu} \boldsymbol{u}, \qquad D_{\mu} = \operatorname{diag}(\mu_0, \cdots, \mu_{N_p-1}),$$

where \hat{p}^{d} is the discrete momentum operator.

We denote by Πu the L^2 projection onto S_p , namely,

$$(\Pi u, v) = (u, v), \quad v \in S_n.$$

One can verify that

$$\Pi u(p) = \sum_{l=0}^{N_p - 1} \hat{u}_l \phi_l(p), \quad \hat{u}_l = \frac{1}{b - a} \int_a^b u(p) e^{-i\mu_l(p - a)} dp, \quad l = 0, \dots, N_p - 1.$$

For the projection, we have the following approximation error in the maximum norm.

Lemma 4.1. For any m > 1/2 and $u \in C_p^m[a,b]$, there exists a positive constant C, independent of N_p , such that

$$||u - \Pi u||_{L^{\infty}} \le C \left(\frac{b-a}{N_p}\right)^{m-1/2} ||u^{(m)}||_{L^2[a,b]}.$$

Here, $C_p^m[a,b]$ consists of functions with derivatives of order up to (m-1) being periodic on [a,b].

Proof. The proof was given in [21, Theorem 2.12] for $[a, b] = [0, 2\pi]$. Scaling argument yields the desired result.

Let $\mathbf{v}(t,p) = [v_1(t,p), \cdots, v_N(t,p)]^T$ be the solution to (3.2). The spectral discretization of $v_i(t,p)$ is

$$v_{i,h}(t,p) = \sum_{l=0}^{N_p-1} \tilde{v}_{i,l,h}(t)\phi_l(p), \qquad i = 1, \dots, N,$$

where we use the subscript h to denote the numerical solution for (3.2). The approximate solution is then given by $\mathbf{v}_h(t,p) = [v_{1,h}(t,p), \cdots, v_{N,h}(t,p)]^T$, which can be written as

$$\mathbf{v}_h(t,p) = \sum_{l=0}^{N_p-1} \tilde{\mathbf{v}}_{l,h}(t)\phi_l(p), \qquad \tilde{\mathbf{v}}_{l,h}(t) = \frac{1}{N_p} \sum_{k=0}^{N_p-1} \mathbf{v}_h(t,p_k) e^{-i\mu_l(p_k-a)}.$$
(4.2)

Let the vector \mathbf{w}_h be the collection of the function \mathbf{v}_h at the grid points, defined more precisely as

$$\boldsymbol{w}_h(t) = \sum_{k,i} v_{i,h}(t,p_k)|k,i\rangle = [\boldsymbol{v}_h(t,p_0);\cdots;\boldsymbol{v}_h(t,p_{N_p-1})].$$

Accordingly, we define

$$\tilde{\boldsymbol{w}}_h(t) = \sum_{l,i} \tilde{v}_{i,l,h}(t)|l,i\rangle = [\tilde{\boldsymbol{v}}_{0,h}(t);\cdots;\tilde{\boldsymbol{v}}_{N_p-1,h}(t)],$$

with ";" indicating the straightening of $\{\tilde{v}_{i,h}\}_{i\geq 1}$ into a column vector. One can find that $w_h(t) = (\Phi \otimes I_{N\times N})\tilde{w}_h(t)$. The equation in (3.2) is then transformed into

$$\begin{cases}
\frac{\mathrm{d}}{\mathrm{d}t} \boldsymbol{w}_h(t) = \mathrm{i}(P_\mu \otimes A) \boldsymbol{w}_h(t), \\
\boldsymbol{w}_h(0) = \boldsymbol{\zeta} \otimes \boldsymbol{b},
\end{cases} (4.3)$$

where $\boldsymbol{\zeta} = [\zeta(p_0), \cdots, \zeta(p_{N_p-1})]^T$. In terms of $\tilde{\boldsymbol{w}}_h = (\Phi^{-1} \otimes I) \boldsymbol{w}_h$, one gets the following Hamiltonian system:

$$\begin{cases}
\frac{\mathrm{d}}{\mathrm{d}t}\tilde{\boldsymbol{w}}_h(t) = \mathrm{i}(D_{\mu}\otimes A)\tilde{\boldsymbol{w}}_h(t), \\
\tilde{\boldsymbol{w}}_h(0) = \tilde{\boldsymbol{\zeta}}\otimes \boldsymbol{b}, \quad \tilde{\boldsymbol{\zeta}} = \Phi^{-1}\boldsymbol{\zeta}.
\end{cases}$$
(4.4)

4.2 Truncation of the integral

The solution to (4.4) can be written as

$$\tilde{\boldsymbol{w}}_h(t) = e^{i(D_\mu \otimes A)t} \tilde{\boldsymbol{w}}_h(0), \tag{4.5}$$

which gives

$$\boldsymbol{w}_h(t) = [\boldsymbol{v}_h(t, p_0); \cdots; \boldsymbol{v}_h(t, p_{N_p-1})] = (\Phi \otimes I) e^{\mathrm{i}(D_\mu \otimes A)t} \tilde{\boldsymbol{w}}_h(0).$$

According to Theorem 3.1, we can recover the approximate solution to the linear systems problem by projecting $\mathbf{w}_h(t)$ onto $|p=0\rangle$ and truncate the integral as

$$\boldsymbol{x}_T = \int_0^T \Pi_* \boldsymbol{w}_h(t) dt = \int_0^T \boldsymbol{v}_h(t, 0) dt, \tag{4.6}$$

where $\Pi_* = |k_*\rangle\langle k_*| \otimes I$ with k_* satisfying $p_{k_*} = 0$. It should be noted that the periodic boundary condition must be maintained throughout the duration, so a stronger condition on R should be imposed. Let $\bar{\boldsymbol{v}} = U^{\dagger}\boldsymbol{v}$. Then, the convection system (3.2) can be diagonalized as

$$\begin{cases} \frac{\mathrm{d}}{\mathrm{d}t} \bar{\boldsymbol{v}}(t,p) = \Lambda \partial_p \bar{\boldsymbol{v}}(t,p), \\ \bar{\boldsymbol{v}}(0,p) = \zeta(p) \bar{\boldsymbol{b}}, & \bar{\boldsymbol{b}} = U^{\dagger} \boldsymbol{b}. \end{cases}$$

The solution is $\bar{v}_i(t,p) = \zeta(p + \lambda_i t)\bar{b}_i$ $(1 \leq i \leq N)$, where \bar{v}_i and \bar{b}_i are the *i*-th entry of \bar{v} and \bar{b} , respectively. For this reason, we require

$$\zeta^{(m-1)}(\pm \pi R + \lambda_i t) \approx 0, \qquad t \in [0, T], \qquad i \ge 1, \qquad m \ge 0.$$

Here we also require that the derivatives of order up to (m-1) are approximately zero in view of the error estimation. Since $\zeta(p)$ is an odd function with rapid decay, we can require that

$$R'(t) := \pi R - |\lambda|_{\max} t \tag{4.7}$$

is sufficiently large.

The criterion of the truncation for T is presented below.

Theorem 4.1. Let $p \in [-\pi R, \pi R]$ with R > 0 satisfying $\zeta^{(m-1)}(R') \approx 0$, where R' is defined in (4.7) and $\zeta(p)$ is defined in Theorem 3.1. Then for any m > 1/2, there holds

$$|\boldsymbol{v}(\cdot, p_k) - \boldsymbol{v}_h(\cdot, p_k)| \lesssim \left(\frac{2\pi R}{N_p}\right)^{m-1/2} |\zeta|_m ||\boldsymbol{b}||, \quad k = 0, 1, \dots, N_p - 1.$$

$$(4.8)$$

Suppose that $v_h(t,0)$ is a vector given by the solution of (4.3) and define x_T by (4.6), where

$$T = \Theta\left(\frac{\kappa}{\|A\|} \sqrt{2\log \frac{2\kappa}{\|A\|\delta}}\right).$$

Under the condition of Theorem 3.1, there holds

$$\|\boldsymbol{x} - \boldsymbol{x}_T\| \lesssim \delta \|\boldsymbol{b}\| \tag{4.9}$$

if we choose $m \sim \frac{2\log(T/\delta)}{\log(\log(1/\delta))}$, $R \sim \kappa poly\log(\kappa/\delta)$, and

$$N_p \sim 2\pi R |\zeta|_m^{1/m} \sqrt{\log(1/\delta)} \sim |\zeta|_m^{1/m} \kappa \operatorname{poly} \log(\kappa/\delta).$$

Proof. (1) We first prove (4.8). For the exact solution \boldsymbol{v} to (3.2), the L^2 projection $\Pi \boldsymbol{v}$ is defined as $\Pi \boldsymbol{v} = [\Pi v_1, \dots, \Pi v_n]^T$. We can write it as

$$\Pi \mathbf{v}(t,p) = \sum_{l=0}^{N_p-1} \hat{\mathbf{v}}_l(t) \phi_l(p), \quad \hat{\mathbf{v}}_l(t) = \frac{1}{b-a} \int_a^b \mathbf{v}(t,p) e^{-i\mu_l(p-a)} dp, \quad l = 0, \dots, N_p - 1.$$
 (4.10)

By the triangle inequality, the error can be split as

$$|\boldsymbol{v}(\cdot, p_k) - \boldsymbol{v}_h(\cdot, p_k)| \le |\boldsymbol{v}(\cdot, p_k) - \Pi \boldsymbol{v}(\cdot, p_k)| + |\Pi \boldsymbol{v}(\cdot, p_k) - \boldsymbol{v}_h(\cdot, p_k)|.$$

Noting that $\zeta^{(m)}(R') \approx 0$, where R' = R'(t) is defined in (4.7), one can easily find that $\mathbf{v}^{(m)}(t,p) \approx \mathbf{0}$ at p = a, b through diagonalization, where $a = -\pi R$ and $b = \pi R$. This implies that each entry of $\mathbf{v}(t,p)$ can be treated as a function in $C_p^m[a,b]$ for any $m \geq 0$.

For the first term on the right-hand side, by Lemma 4.1, there holds

$$|\mathbf{v}(\cdot, p_k) - \Pi \mathbf{v}(\cdot, p_k)| \le \|\mathbf{v}(\cdot, p) - \Pi \mathbf{v}(\cdot, p)\|_{L^{\infty}} \lesssim \left(\frac{b - a}{N_p}\right)^{m - 1/2} \|\mathbf{v}^{(m)}(\cdot, p)\|_{L^{2}[a, b]}$$
$$\lesssim \left(\frac{b - a}{N_p}\right)^{m - 1/2} \|\zeta^{(m)}\|_{L^{2}[a, b]} \|\mathbf{b}\| = \left(\frac{b - a}{N_p}\right)^{m - 1/2} |\zeta|_{m} \|\mathbf{b}\|.$$

For the second term, by definition, one gets

$$\Pi oldsymbol{v}(\cdot,p) - oldsymbol{v}_h(\cdot,p) = \sum_{l=0}^{N_p-1} (\hat{oldsymbol{v}}_l(t) - ilde{oldsymbol{v}}_{l,h}(t)) \phi_l(p).$$

The evolution of $\tilde{v}_{l,h}(t)$ is given in (4.4). For each $\hat{v}_l(t)$, we obtain from its definition and (3.2) that

$$\frac{\mathrm{d}}{\mathrm{d}t}\hat{\mathbf{v}}_l(t) = \mathrm{i}\mu_l A\hat{\mathbf{v}}_l(t), \quad l = 0, \cdots, N_p - 1.$$

Let $\hat{\boldsymbol{w}}(t) = \sum_{l,i} \hat{v}_{i,l}(t) | l,i \rangle = [\hat{\boldsymbol{v}}_0(t); \cdots; \hat{\boldsymbol{v}}_{N_p-1}(t)]$. The above system can be rewritten as

$$\frac{\mathrm{d}}{\mathrm{d}t}\hat{\boldsymbol{w}}(t) = \mathrm{i}(D_{\mu} \otimes A)\hat{\boldsymbol{w}}(t).$$

Introducing the vector

$$\boldsymbol{w}_{\pi}(t) = (\Phi \otimes I)\hat{\boldsymbol{w}}(t) = [\Pi \boldsymbol{v}(t, p_0); \cdots; \Pi \boldsymbol{v}(t, p_{N_p-1})],$$

we have

$$\begin{cases} \frac{\mathrm{d}}{\mathrm{d}t} \boldsymbol{w}_{\pi}(t) = \mathrm{i}(P_{\mu} \otimes A) \boldsymbol{w}_{\pi}(t), \\ \boldsymbol{w}_{\pi}(0) = \boldsymbol{\zeta}_{\pi} \otimes \boldsymbol{b}, \end{cases}$$

where $\zeta_{\pi} = [\Pi \zeta(p_0); \cdots; \Pi \zeta(p_{N_p-1})]^T$. Let $\boldsymbol{e}_h(t) = \boldsymbol{w}_h(t) - \boldsymbol{w}_{\pi}(t)$. Then,

$$\begin{cases} \frac{\mathrm{d}}{\mathrm{d}t} \boldsymbol{e}_h(t) = \mathrm{i}(P_{\mu} \otimes A) \boldsymbol{e}_h(t), \\ \boldsymbol{e}_h(0) = (\boldsymbol{\zeta} - \boldsymbol{\zeta}_{\pi}) \otimes \boldsymbol{b}, \end{cases}$$

which gives $e_h(t) = e^{i(P_\mu \otimes A)t} e_h(0)$ and

$$|\boldsymbol{v}_h(\cdot,p_k) - \Pi \boldsymbol{v}(\cdot,p_k)| \leq \|\boldsymbol{e}_h(t)\| = \|\boldsymbol{\zeta} - \boldsymbol{\zeta}_{\pi}\| \cdot \|\boldsymbol{b}\| \lesssim \left(\frac{b-a}{N_p}\right)^{m-1/2} |\zeta|_m \|\boldsymbol{b}\|.$$

(2) By definition,

$$\mathbf{x} - \mathbf{x}_T = \int_0^\infty \mathbf{v}(t,0) dt - \int_0^T \mathbf{v}_h(t,0) dt$$
$$= \left(\int_0^\infty \mathbf{v}(t,0) dt - \int_0^T \mathbf{v}(t,0) dt \right) + \left(\int_0^T \mathbf{v}(t,0) dt - \int_0^T \mathbf{v}_h(t,0) dt \right)$$
$$=: I_1 + I_2.$$

For I_1 , the diagonalization of A yields

$$||I_1|| = \left\| \int_0^\infty \int_{\mathbb{R}} \zeta(k) e^{-ikAs} dk ds \boldsymbol{b} - \int_0^T \int_{\mathbb{R}} \zeta(k) e^{-ikAs} dk ds \boldsymbol{b} \right\|$$

$$= \max_j \left| \int_0^\infty \hat{\varphi}(\lambda_j s) ds - \int_0^T \hat{\varphi}(\lambda_j s) ds \right| ||\boldsymbol{b}||$$

$$= \max_j \frac{1}{|\lambda_j|} e^{-(\lambda_j T)^2/2} ||\boldsymbol{b}|| \le \frac{\delta}{2} ||\boldsymbol{b}||,$$

so we can set $T = \Theta(\frac{\kappa}{\|A\|} \sqrt{2 \log \frac{2\kappa}{\|A\|\delta}})$. For I_2 , using the estimation established in the first step, we obtain

$$||I_2|| \lesssim \left(\frac{2\pi R}{N_p}\right)^{m-1/2} |\zeta|_m T ||\boldsymbol{b}||.$$

The condition $\zeta^{(i)}(R') \approx 0$ or $\zeta^{(i)}(R') \leq \delta$ $(i \leq m-1)$ implies that we can choose

$$\pi R = |\lambda|_{\max} T + \text{poly} \log(1/\delta) = \mathcal{O}(\kappa \text{poly} \log(\kappa/\delta)).$$

For m > 1/2, assuming that

$$\left(\frac{2\pi R}{N_p}\right)^{m-1/2} |\zeta|_m T \le \left(\frac{2\pi R}{N_p}\right)^m |\zeta|_m T = \delta,$$

we find

$$N_p \sim 2\pi R |\zeta|_m^{1/m} T^{1/m} \delta^{-1/m}$$
.

By solving $(T/\delta)^{1/m} \sim \sqrt{\log(1/\delta)}$, one has

$$N_p \sim 2\pi R |\zeta|_m^{1/m} \sqrt{\log(1/\delta)} \sim |\zeta|_m^{1/m} \kappa \operatorname{poly} \log(\kappa/\delta) \quad \text{if} \quad m \sim \frac{2\log(T/\delta)}{\log(\log(1/\delta))}. \tag{4.11}$$

This completes the proof.

Remark 4.1. The step size Δp for the variable p satisfies

$$||D_{\mu}|| = \max_{l} |\mu_{l}| \lesssim \frac{1}{\Delta p} = \frac{N_{p}}{2\pi R} = \mathcal{O}(|\zeta|_{m}^{1/m} \sqrt{\log(1/\delta)}).$$

4.3 Discretization of the truncated integral

Let $U(A,t) = e^{i(D_{\mu} \otimes A)t}$. We have

$$\boldsymbol{x} \approx \boldsymbol{x}_T = \Pi_*(\Phi \otimes I)g(A)\tilde{\boldsymbol{w}}_h(0), \qquad g(A) = \int_0^T U(A,t)dt$$
 (4.12)

for sufficiently large T, where Π_* is the projector defined in (4.6).

To present an explicit algorithm, we need to express the truncated integral as a finite sum using numerical integration. Let $t_m = m\tau$ for $m = 0, 1, \dots, N_t$, where $N_t = T/\tau$ and τ is the step size. We use composite Gaussian quadrature to discretize the variable t and obtain

$$g(A) = \sum_{m=0}^{N_t - 1} \int_{m\tau}^{(m+1)\tau} U(A, t) dt \approx \sum_{m=0}^{N_t - 1} \sum_{q=0}^{Q - 1} c_{m,q} e^{i(D_{\mu} \otimes A)t_{m,q}} =: p(A),$$
(4.13)

where, on each interval $[m\tau, (m+1)\tau]$, we use Gaussian quadrature with Q nodes. The $t_{m,q}$'s are the Gaussian nodes, $c_{m,q} = w_q$ and w_q 's are the Gaussian weights (which do not depend on the choice of m). The resulting approximation for (4.12) is defined as

$$\boldsymbol{x}_T^{\mathrm{d}} =: \Pi_*(\Phi \otimes I) p(A) \tilde{\boldsymbol{w}}_h(0). \tag{4.14}$$

To measure the accuracy of the approximation, we first introduce the quadrature error described as follows.

Lemma 4.2. Let A be a Hermitian matrix. Suppose that $f(\cdot, x)$ is a function in $C^{2Q}[a, b]$ with respect to x and f(A, x) is well-defined. Let w_q and x_q be the Gaussian quadrature weights and points on [a, b] for $q = 0, 1, \dots, Q - 1$. There there holds

$$\left\| \int_{a}^{b} f(A, x) dx - \sum_{q=0}^{Q-1} w_q f(A, x_q) \right\| \le \frac{(b-a)^{2Q+1} (Q!)^4}{(2Q+1)[(2Q)!]^3} \max_{x \in [a, b]} \|f^{(2Q)}(A, x)\|,$$

where the subscript (q) refers to the qth-order partial derivative with respect to x.

Proof. Since A is a Hermitian matrix, there exists a unitary matrix U such that $A = U\Lambda U^{-1}$, where $\Lambda = \text{diag}(\lambda_1, \dots, \lambda_n)$, which yields

$$\left\| \int_{a}^{b} f(A, x) dx - \sum_{q=0}^{Q-1} w_{q} f(A, x_{q}) \right\| = \left\| \int_{a}^{b} f(\Lambda, x) dx - \sum_{q=0}^{Q-1} w_{q} f(\Lambda, x_{q}) \right\|.$$

According to Chapter 5 of [22], there exists $\xi_j \in (a, b)$ such that

$$\int_{a}^{b} f(\lambda_{j}, x) dx - \sum_{q=0}^{Q-1} w_{q} f(\lambda_{j}, x_{q}) = \frac{(b-a)^{2Q+1} (Q!)^{4}}{(2Q+1)[(2Q)!]^{3}} f^{(2Q)}(\lambda_{j}, \xi_{j}).$$

Therefore,

$$\int_{a}^{b} f(\Lambda, x) dx - \sum_{q=0}^{Q-1} w_{q} f(\Lambda, x_{q}) = \frac{(b-a)^{2Q+1} (Q!)^{4}}{(2Q+1)[(2Q)!]^{3}} \begin{bmatrix} f^{(2Q)}(\lambda_{1}, \xi_{1}) & & \\ & \ddots & \\ & & f^{(2Q)}(\lambda_{n}, \xi_{n}) \end{bmatrix},$$

which implies the desired estimate.

Lemma 4.3. Let p(A) be defined in (4.13). Under the condition of Theorem 4.1, the quadrature error can be bounded as

$$||g(A) - p(A)|| \le \delta \tag{4.15}$$

when we choose

$$\tau = \frac{1}{\|D_{\mu} \otimes A\|}, \quad Q = \Theta\left(\log \frac{T}{\delta}\right).$$

Proof. The error can be decomposed as

$$||g(A) - p(A)|| \le ||g(A) - \sum_{m=0}^{N_t - 1} \sum_{q=0}^{Q-1} c_{m,q} e^{i(D_{\mu} \otimes A)t_{m,q}}|| =: I.$$

By Lemma 4.2,

$$\left\| \int_0^T U(A,t) dt - \sum_{m=0}^{N_t - 1} \sum_{q=0}^{Q-1} c_{m,q} U(A,t_{m,q}) \right\| \le \frac{N_t \tau^{2Q+1}(Q!)^4}{(2Q+1)[(2Q)!]^3} \max_t \| U^{(2Q)}(A,t) \|.$$

It is simple to find that

$$\max_{t} ||U^{(2Q)}(A, t)|| \le ||D_{\mu} \otimes A||^{2Q},$$

which gives

$$I \le T \frac{\tau^{2Q}(Q!)^4}{(2Q+1)[(2Q)!]^3} \|D_{\mu} \otimes A\|^{2Q}.$$

If we choose $\tau = \frac{1}{\|D_{\mu} \otimes A\|}$, then

$$I \le \frac{T(Q!)^4}{(2Q+1)[(2Q)!]^3}.$$

Therefore, we obtain $I \leq \delta$ by choosing Q such that

$$\frac{(Q!)^4}{(2Q+1)[(2Q)!]^3} \le \frac{\delta}{T}.$$

As before, it suffices to choose $Q = \Theta(\log \frac{T}{\delta})$, which completes the proof.

Combining the result in Theorem 4.1, we are ready to obtain the approximation error.

Theorem 4.2. Let A be an invertible Hermitian matrix. Suppose that \mathbf{x} is the exact solution of $A\mathbf{x} = \mathbf{b}$ and \mathbf{x}_T^d is the numerical solution defined in (4.14), respectively. Under the condition of Theorem 4.1, if we choose

$$T = \Theta\left(\frac{\kappa}{\|A\|} \sqrt{2 \log \frac{2\kappa}{\|A\|\delta}}\right), \qquad \tau = \frac{T}{N_t} = \frac{1}{\|D_{\mu} \otimes A\|}, \qquad Q = \Theta\left(\log \frac{T}{\delta}\right),$$

then there holds

$$\|\boldsymbol{x} - \boldsymbol{x}_T^d\| \lesssim \delta \log^{1/4}(1/\delta) \|\boldsymbol{b}\|.$$

Proof. According to Eq. (4.15) in Lemma 4.3, we obtain from $\|\tilde{\boldsymbol{w}}_h(0)\| = \|\boldsymbol{w}_h(0)\| = \|\boldsymbol{\zeta}\| \|\boldsymbol{b}\|$ that

$$\|\boldsymbol{x}_T - \boldsymbol{x}_T^{\mathrm{d}}\| \le \|g(A) - p(A)\|\|\tilde{\boldsymbol{w}}_h(0)\| = \|g(A) - p(A)\|\|\boldsymbol{w}_h(0)\| \le \delta \|\boldsymbol{\zeta}\|\|\boldsymbol{b}\|$$

This along with the equation (4.9) of Theorem 4.1 yields

$$\|x - x_T^{\mathrm{d}}\| \le \|x - x_T\| + \|x_T - x_T^{\mathrm{d}}\| \le \delta(\|\zeta\| + 1)\|b\|.$$

According to Remark 4.1, there holds

$$\|\boldsymbol{\zeta}\| \leq \left(\frac{1}{\Delta p} \int_{\mathbb{R}} |\zeta(p)|^2 \mathrm{d}p\right)^{1/2} = \left(\frac{1}{\Delta p} \frac{\sqrt{2}}{2}\right)^{1/2} = \mathcal{O}(\log^{1/4}(1/\delta)).$$

This completes the proof.

4.4 Linear combination of unitaries

For simplicity we rewrite the summation in (4.13) by a single index as

$$p(A) = \sum_{m=0}^{N_t - 1} \sum_{q=0}^{Q-1} c_{m,q} e^{i(D_\mu \otimes A)t_{m,q}} =: \sum_{j=0}^{M-1} \alpha_j U_j,$$
(4.16)

where

$$U_j = e^{i(D_\mu \otimes A)t_j} = (e^{i(D_\mu \otimes A)\tau})^j$$

It is evident that $M \leq N_t Q$ since we have collected the like terms. Moreover, the initial data $\tilde{\boldsymbol{w}}_h(0)$ is given in (4.4).

In the following we will present the details on how to apply the LCU technique to effectively prepare the solution state for Ax = b. To this end, we need to pre-construct the following oracles.

• The coefficient oracles

$$O_{\text{coef}}: |0^{n_a}\rangle \to \frac{1}{\sqrt{\|\boldsymbol{\alpha}\|_1}} \sum_{j=0}^{M-1} \sqrt{\alpha_j} |j\rangle, \qquad M = 2^{n_a},$$

with $\alpha = (\alpha_0, \dots, \alpha_{M-1})$ and $\|\alpha\|_1 = \alpha_0 + \dots + \alpha_{M-1}$. It is obvious that

$$\|\alpha\|_1 = \sum_{m=0}^{N_t-1} \sum_{q=0}^{Q-1} |c_{m,q}| = \mathcal{O}(T),$$

where the last equality is obtained from $\sum_{q,m} |c_{q,m}| = \int_0^T dt = T$.

• The select oracle

$$\operatorname{SEL}_{A} = \sum_{j=0}^{M-1} |j\rangle\langle j| \otimes U_{j}, \qquad U_{j} = (e^{\mathrm{i}(D_{\mu}\otimes A)\tau})^{j}.$$

• The state preparation oracle

$$O_w: |0^{n_w}\rangle \to |\tilde{w}_h(0)\rangle,$$

where $|\tilde{w}_h(0)\rangle$ is the quantum state for $\tilde{\boldsymbol{w}}_h(0)$.

Theorem 4.3. Let A be an invertible Hermitian matrix and assume that \mathbf{x} is the solution to $A\mathbf{x} = \mathbf{b}$. Then there exists a quantum algorithm that prepares an ε -approximation of the state $|x\rangle = \mathbf{x}/\|\mathbf{x}\|$ with $\Omega(1)$ success probability and a flag indicating success, using $\mathcal{O}((\|\mathbf{\alpha}\|_1\|\zeta\|)/\xi)$ queries to the coefficient oracles O_{coef} , the select oracle SEL_A and the state preparation oracle O_w , where

$$\|\boldsymbol{\alpha}\|_1 = \mathcal{O}(T) = \mathcal{O}\left(\frac{\kappa}{\|A\|}\sqrt{2\log\frac{2\kappa}{\|A\|\delta}}\right), \qquad \xi = \|A^{-1}|b\rangle\|, \quad |b\rangle = \boldsymbol{b}/\|\boldsymbol{b}\|,$$

with
$$\|\boldsymbol{\zeta}\| = \mathcal{O}(\log^{1/4}(1/\delta))$$
 and $\delta = \frac{\varepsilon \xi}{\log^{1/4}(1/(\varepsilon \xi))}$.

Proof. The procedure of preparing an approximation of the state proportional to

$$\mathbf{w}_{\mathrm{int}} := \int_0^T \mathbf{w}_h(t) \mathrm{d}t = \sum_{k=0}^{N_p-1} |k\rangle \otimes \int_0^T \mathbf{v}_h(t, p_k) \mathrm{d}t = (\Phi \otimes I)g(A)\tilde{\mathbf{w}}_h(0)$$

is given as follows:

$$|0^{n_{a}}\rangle \otimes |0^{n_{w}}\rangle \qquad \frac{O_{\operatorname{coef}} \otimes I^{\otimes n_{w}}}{\sqrt{\|\boldsymbol{\alpha}\|_{1}}} \sum_{j=0}^{M-1} \sqrt{\alpha_{j}} |j\rangle \otimes |0^{n_{w}}\rangle$$

$$\frac{I^{\otimes n_{a}} \otimes O_{w}}{\sqrt{\|\boldsymbol{\alpha}\|_{1}}} \sum_{j=0}^{M-1} \sqrt{\alpha_{j}} |j\rangle \otimes |\tilde{w}_{h}(0)\rangle$$

$$\frac{\operatorname{SEL}_{A}}{\sqrt{\|\boldsymbol{\alpha}\|_{1}}} \sum_{j=0}^{M-1} \sqrt{\alpha_{j}} |j\rangle \otimes U_{j} |\tilde{w}_{h}(0)\rangle$$

$$\frac{O_{\operatorname{coef}}^{\dagger} \otimes I^{\otimes n_{w}}}{\|\boldsymbol{\alpha}\|_{1}} |0^{n_{a}}\rangle \otimes \sum_{j=0}^{M-1} \alpha_{j} U_{j} |\tilde{w}_{h}(0)\rangle + |\bot\rangle$$

$$\frac{I^{\otimes n_{a}} \otimes \Phi \otimes I^{\otimes n}}{\|\boldsymbol{\alpha}\|_{1}} |0^{n_{a}}\rangle \otimes (\Phi \otimes I) p(A) |\tilde{w}_{h}(0)\rangle + |\bot'\rangle.$$

Denote by V the resulting unitary operator. Then,

$$|0^{n_a}\rangle \otimes |0^{n_w}\rangle \xrightarrow{V} \frac{1}{\|\boldsymbol{\alpha}\|_1} |0^{n_a}\rangle \otimes (\Phi \otimes I) p(A) |\tilde{w}_h(0)\rangle + |\perp'\rangle$$

$$= \frac{1}{\|\boldsymbol{\alpha}\|_1 \|\tilde{\boldsymbol{w}}_h(0)\|} |0^{n_a}\rangle \otimes \boldsymbol{w}_{\text{int}}^{\text{d}} + |\perp'\rangle,$$

where $w_{\text{int}}^{\text{d}}$ is the approximation of w_{int} obtained through numerical integration.

The final approximate state $|x_T^d\rangle$ corresponding to $\boldsymbol{x}_T^d = \Pi_* \boldsymbol{w}_{\text{int}}^d$ is obtained by projection. Using the inequality $\|\frac{\boldsymbol{x}}{\|\boldsymbol{x}\|} - \frac{\boldsymbol{y}}{\|\boldsymbol{y}\|}\| \le 2\frac{\|\boldsymbol{x}-\boldsymbol{y}\|}{\|\boldsymbol{x}\|}$ for two vectors $\boldsymbol{x}, \boldsymbol{y}$ and using the estimate in Theorem 4.2, we can bound the error in the quantum state after a successful measurement as

$$\||x\rangle - |x_T^{\mathrm{d}}\rangle\| \le 2 \frac{\|\boldsymbol{x} - \boldsymbol{x}_T^{\mathrm{d}}\|}{\|\boldsymbol{x}\|} \lesssim 2 \frac{\delta \sqrt{\log(1/\delta)} \|\boldsymbol{b}\|}{\|\boldsymbol{x}\|}.$$

Therefore, we can require that

$$\frac{\delta \log^{1/4}(1/\delta) \|\boldsymbol{b}\|}{\|\boldsymbol{x}\|} \le \varepsilon \quad \text{or} \quad \delta \log^{1/4}(1/\delta) \le \frac{\varepsilon \|\boldsymbol{x}\|}{\|\boldsymbol{b}\|} = \varepsilon \xi,$$

which implies

$$\delta \le \frac{\varepsilon \xi}{\log^{1/4}(1/(\varepsilon \xi))}$$

since $\delta \leq \varepsilon \xi$ if $0 < \delta < 1$. The state $|w_{\rm int}^{\rm d}\rangle$ is obtained by measuring the state in the flow map and obtaining all 0 in the other qubits. The likelihood of acquiring this approximate state is

$$P_w = \left(\frac{\|\boldsymbol{w}_{\text{int}}^{\text{d}}\|}{\|\boldsymbol{\alpha}\|_1 \|\tilde{\boldsymbol{w}}_h(0)\|}\right)^2.$$

To get the final approximate state $|x_T^d\rangle$, we need to perform the projection onto $|k_*\rangle$ as shown in (4.6), with the probability given by

$$P_x = \left(\frac{\|\boldsymbol{w}_*^{\mathrm{d}}\|}{\|\boldsymbol{w}_{\mathrm{int}}^{\mathrm{d}}\|}\right)^2,$$

where $\boldsymbol{w}_*^{\mathrm{d}}$ is the numerical approximation of $\int_0^T \boldsymbol{v}_h(t,0) \mathrm{d}t = \boldsymbol{x}_T$. The overall probability is

$$P_r = \left(\frac{\|\boldsymbol{w}_*^{\mathrm{d}}\|}{\|\boldsymbol{\alpha}\|_1 \|\boldsymbol{w}_h(0)\|}\right)^2.$$

The success probability can be raised to $\Omega(1)$ by using $\mathcal{O}(g)$ rounds of amplitude amplification, where

$$g = \frac{\|\boldsymbol{\alpha}\|_1 \|\boldsymbol{w}_h(0)\|}{\|\boldsymbol{w}_*^{\mathrm{d}}\|} = \frac{\|\boldsymbol{\alpha}\|_1 \|\boldsymbol{\zeta}\| \|\boldsymbol{b}\|}{\|\boldsymbol{w}_*^{\mathrm{d}}\|} \approx \frac{\|\boldsymbol{\alpha}\|_1 \|\boldsymbol{\zeta}\| \|\boldsymbol{b}\|}{\|\boldsymbol{x}_T\|} \approx \frac{\|\boldsymbol{\alpha}\|_1 \|\boldsymbol{\zeta}\| \|\boldsymbol{b}\|}{\|\boldsymbol{x}\|} = \mathcal{O}\Big(\frac{T\|\boldsymbol{\zeta}\|}{\|A^{-1}|b\rangle\|}\Big).$$

The proof is finished by combining the result in Theorem 4.2.

Thus, our algorithm for query complexity is consistent with that presented in [4], implying that the final time complexity will exhibit quadratic dependence on the condition number $\kappa(A)$ if we include the cost of the Hamiltonian simulation $U(A,t) = e^{i(D_{\mu} \otimes A)t}$.

Theorem 4.4. Let A be an invertible Hermitian matrix, and consider the linear system $A\mathbf{x} = \mathbf{b}$. Assume the block encoding of A. Then, there exists a quantum algorithm that prepares an ε -approximation of the state $|\mathbf{x}\rangle$ with $\Omega(1)$ success probability and a flag indicating success, using

$$\mathcal{O}\left(\frac{\kappa^2}{\xi \|A\|} \log^{1.5} \frac{\kappa}{\xi \|A\| \varepsilon}\right), \qquad \xi = \|A^{-1}|b\rangle\|, \tag{4.17}$$

queries to the block-encoding oracle for A and

$$\mathcal{O}\Big(\frac{\kappa}{\xi\|A\|}\log^{0.75}\frac{\kappa}{\xi\|A\|\varepsilon}\Big)$$

queries to the state preparation oracle for b.

Proof. According to Theorem 4.3, we invoke Hamiltonian simulation $\mathcal{O}(g)$ times with $g = \|\boldsymbol{\alpha}\|_1 \|\boldsymbol{\zeta}\|/\xi$. The overall error is at most ε provided each simulation has error $\varepsilon' = \mathcal{O}(\varepsilon/g)$. The query complexity of simulating a Hamiltonian $U(A,t) = e^{i(D_{\mu} \otimes A)t}$ for time t = T with error at most ε' is

$$\mathcal{O}(\|D_{\mu}\|\|A\|T + \log \frac{1}{\varepsilon'}), \qquad \|D_{\mu}\| = \mathcal{O}(\log^{1/4}(1/\delta)).$$

Thus the total query complexity is

$$\mathcal{O}\left(g(\|D_{\mu}\|\|A\|T + \log\frac{1}{\varepsilon'})\right) = \mathcal{O}\left(\frac{\kappa^2}{\xi\|A\|}\log^{1.5}\frac{\kappa}{\xi\|A\|\varepsilon}\right).$$

This completes the proof.

Remark 4.2. The factor $\xi \|A\|$ is invariant under the transformation $A \to cA$, where c is a constant. In the best case scenario that $|b\rangle$ has an $\Omega(1)$ overlap with the left-singular vector of A with respect to the smallest singular value, $\xi \|A\| = \|A^{-1}|b\rangle \|\|A\| = \Omega(\kappa)$ and hence the nearly linear run time $\mathcal{O}(\kappa \log^{1.5}(1/\varepsilon))$ is obtained with respect to the condition number κ .

Remark 4.3. In (4.11), we can replace $\sqrt{\log(1/\delta)}$ with $\log^{1/r}(1/\delta)$ if $m \sim \frac{r \log(T/\delta)}{\log(\log(1/\delta))}$, which implies that we can replace $\log^{1.5}$ in (4.17) by $\log^{1+1/r}$.

5 Applications

In this section, we present several numerical tests to validate the correctness of the proposed method. We focus on testing the kernel function given in (2.2) (or the one given in Remark 2.1), as the kernel function $e^{-|p|}$ does not provide optimal error estimates due to its mere continuity. Unless otherwise specified, the domain for the auxiliary variable p is chosen as $[-\pi R, \pi R]$ with R = 15, and we take $N_p = 2^9$ for the discrete Fourier transform. Note that in a classical computer, we can rewrite (4.4) as a system of decoupled ODEs given by

$$\begin{cases} \frac{\mathrm{d}}{\mathrm{d}t} \tilde{\boldsymbol{v}}_{l,h}(t) = \mathrm{i}\mu_l A \tilde{\boldsymbol{v}}_{l,h}(t), \\ \tilde{\boldsymbol{v}}_{l,h}(0) = \tilde{\zeta}_l \boldsymbol{u}_0, \end{cases} \qquad l = 0, 1, \dots, N_p - 1,$$

where $\tilde{\zeta}_l$'s are the entries of $\tilde{\zeta}$.

5.1 A non-symmetric system

Example 5.1. We first consider a non-symmetric linear system, with

$$A = \begin{bmatrix} 1 & 1 & 0 \\ 0 & 1 & 1 \\ 0 & 0 & 1 \end{bmatrix}, \qquad \boldsymbol{b} = \begin{bmatrix} 1 \\ 1 \\ 1 \end{bmatrix}.$$

In this case, we consider the implementation of a dilated linear system, with the coefficient matrix \tilde{A} , the right-hand side $\tilde{\boldsymbol{b}}$, and the solution $\tilde{\boldsymbol{x}}$ given by

$$ilde{A} = egin{bmatrix} O & A \ A^\dagger & O \end{bmatrix}, \quad ilde{m{b}} = egin{bmatrix} m{b} \ m{0} \end{bmatrix}, \quad ilde{m{x}} = egin{bmatrix} m{0} \ m{x} \end{bmatrix}.$$

The exact solution is $\boldsymbol{x} = [1, 0, 1]^T$. For evolution times T = 10 and T = 15, the approximate solutions are given by

$$m{x}_{10} = egin{bmatrix} 0.999960742741313 \\ 0.000031481877145 \\ 0.999982528876265 \end{bmatrix}, \quad m{x}_{15} = egin{bmatrix} 0.9999999999834868 \\ 0.000000000132425 \\ 0.999999999926509 \end{bmatrix}.$$

The errors in the l^2 norm are 5.3268×10^{-5} and 2.2407×10^{-10} , respectively, which demonstrates the accuracy of the Schrödingerization-form algorithm.

5.2 The Poisson equation

Example 5.2. We consider the one-dimensional Poisson equation

$$-u''(x) = f(x), \qquad x \in (a, b) = (0, 1)$$

with Dirichlet boundary conditions. The exact solution is chosen as $u(x) = e^{-x}$.

Let us consider the finite difference discretization. The domain is uniformly divided into M intervals of length $\Delta x = (b-a)/M$. Let $u_i = u(x_i)$ be the evaluation of u at $x_i = a + i\Delta x$ with $i = 0, 1, \dots, M$. The unknown values are u_1, \dots, u_{M-1} . We apply the central difference discretization at $x = x_j$ for $j = 1, \dots, M-1$:

$$-\frac{u_{j-1}-2u_j+u_{j+1}}{\Delta x^2}=f(x_j)=:f_j, \quad j=1,\cdots,M-1.$$

Let $\boldsymbol{u} = [u_1, \cdots, u_{M-1}]^T = \sum_{j=0}^{M-2} u_{j+1} |j\rangle$, where $|j\rangle = [0, 0, \cdots, 0, 1, 0, \cdots, 0]^T \in \mathbb{R}^{M-1}$ is a column vector with the j-th entry being 1. One gets a linear system $A\boldsymbol{u} = \boldsymbol{b}$ with

$$A = -\frac{1}{\Delta x^{2}} \begin{bmatrix} -2 & 1 & & & \\ 1 & -2 & \ddots & & \\ & \ddots & \ddots & \ddots & \\ & & \ddots & -2 & 1 \\ & & & 1 & -2 \end{bmatrix}_{(M-1)\times(M-1)}, \quad \boldsymbol{b} = \begin{bmatrix} f_{1} + u_{0}/\Delta x^{2} \\ f_{2} \\ \vdots \\ f_{M-2} \\ f_{M-1} + u_{M}/\Delta x^{2} \end{bmatrix}.$$
 (5.1)

We first consider the Fourier approach in [4]. One can apply the Gaussian quadrature rule as done in (4.13) with the details omitted. In the numerical test, we take (a, b) = (0, 1) and M = 10. The numerical and exact solutions are depicted in Fig. 1a. We also conduct the test for our approach with the evolution time T = 20. The result is presented in Fig. 1b. It is observed both methods yield satisfactory results.

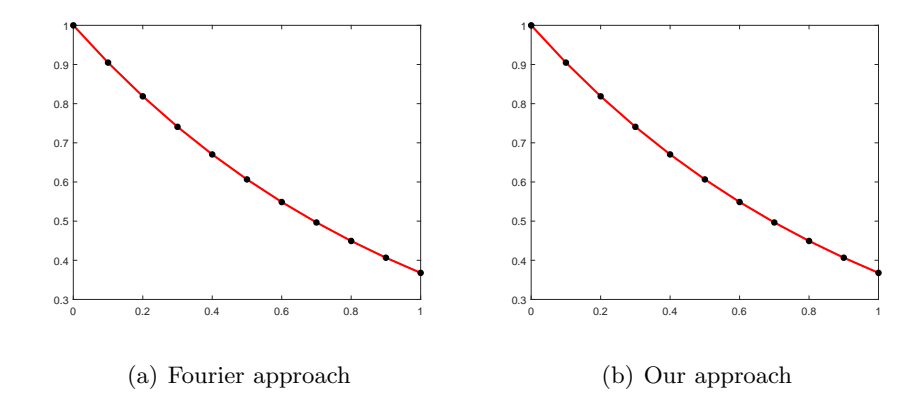


Fig. 1: Finite difference discretization for the Poisson equation in one dimension

Example 5.3. We consider the two-dimensional Poisson equation

$$-\Delta u = f(x), \qquad x \in \Omega = (0,1)^2.$$

The Dirichlet boundary conditions and the right-hand side are chosen such that the exact solution is $u(x,y) = y^2 \sin(\pi x)$.

For this example, we apply the finite element discretization using \mathbb{P}_1 -Lagrange elements. For simplicity, we assume homogeneous boundary condition. The finite element space is defined by

$$V_h := \{ v \in H_0^1(\Omega) : v | K \in \mathbb{P}_1(K), \quad K \in \mathcal{T}_h \}, \tag{5.2}$$

where \mathbb{P}_1 is the space of linear polynomials on a triangular mesh \mathcal{T}_h . Let $\varphi_1, \dots, \varphi_N$ be the basis functions of V_h . The linear system in (1.1) is given by

$$a_{ij} = (\nabla \varphi_j, \nabla \varphi_i), \qquad b_i = (f, \varphi_i), \qquad 1 \le i, j \le N.$$
 (5.3)

For further details, please refer to [23]. In the case of relatively small resulting linear systems, the errors are primarily dominated by the spatial discretization. The results for the three refined meshes are presented in Fig. 2, where we observe that our Schrödingerization-form approach provides satisfactory results. Additionally, the convergence rates in the L^2 and H^1 norms are shown in Fig. 3a. It is evident that the errors in both the L^2 and H^1 norms exhibit second-order and first-order convergence, respectively, which aligns with the standard theoretical predictions in finite element methods.

However, when the resulting linear system becomes relatively large, the evolution time T should be larger than in the previous cases, which in turn increases the domain size for the variable p. If we continue to use the same parameters for the next refinement, the convergence rate deviates significantly from the theoretical prediction, as shown in Fig. 3b. To address this, one can adjust the parameters, for instance by setting T = 50, R = 35, and $N_p = 2^{11}$, which yields satisfactory results again, as shown in Fig. 3c.

5.3 The linear elasticity problem

Example 5.4. The linear elasticity problem is

$$\begin{cases}
-\operatorname{div}\boldsymbol{\sigma} = \boldsymbol{f} & in \quad \Omega, \\
\boldsymbol{u} = \boldsymbol{0} & on \quad \partial\Omega.
\end{cases}$$
(5.4)

The constitutive relation for linear elasticity is $\sigma(\mathbf{u}) = 2\mu \varepsilon(\mathbf{u}) + \lambda(\operatorname{div}\mathbf{u})\mathbf{I}$, where $\sigma = (\sigma_{ij})$ and $\varepsilon = (\varepsilon_{ij})$ are the second order stress and strain tensors, respectively, satisfying $\varepsilon_{ij} = \frac{1}{2}(\partial_i u_j + \partial_j u_i)$, λ and μ are the Lamé constants, \mathbf{I} is the identity matrix, and $\operatorname{div}\mathbf{u} = \partial_1 u_1 + \partial_2 u_2$. The right-hand side \mathbf{f} and the boundary conditions are chosen in such a way that the exact solution is

$$\boldsymbol{u}(x,y) = \begin{bmatrix} \cos(\pi x)\cos(\pi y) \\ \sin(\pi x)\sin(\pi y) \end{bmatrix}.$$

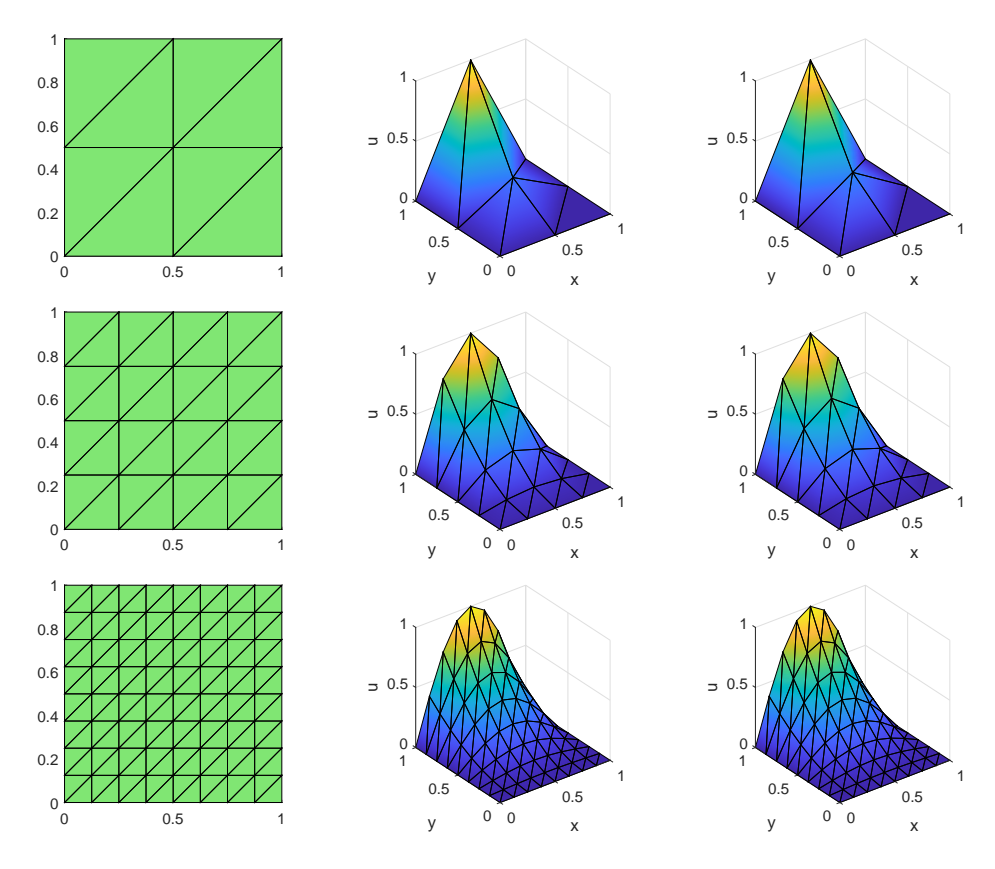


Fig. 2: Exact and numerical solutions for \mathbb{P}_1 -Lagrange elements

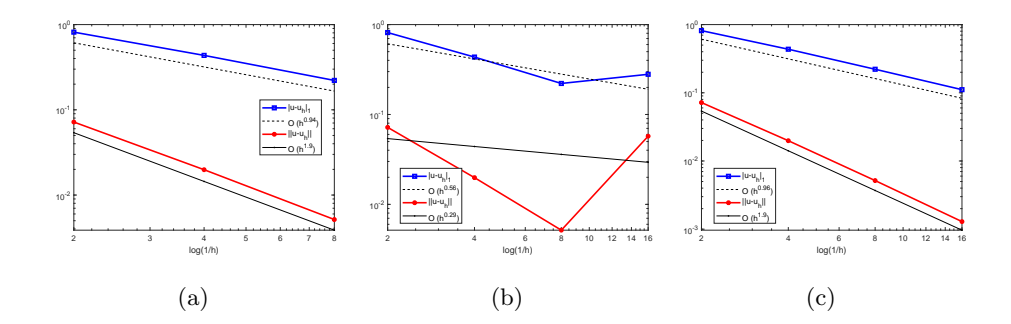


Fig. 3: Convergence rates for \mathbb{P}_1 -Lagrange elements in the L^2 and H^1 norms

We consider the discretization using the Virtual Element Method, which generalizes the standard finite element method to accommodate arbitrary polytopal meshes. For the detailed construction of the numerical method, we refer the reader to [24]. The exact and numerical solutions for the linear virtual element method with 32 polygons are shown in Fig. 2, where only $u_1(x, y)$ is presented. From this, we observe that the Schrödingerization-form approach provides a good match with the exact solution.

5.4 The radiative transfer equation

The steady-state radiative transfer equation can be expressed as

$$\boldsymbol{\omega} \cdot \nabla u(\boldsymbol{x}, \boldsymbol{\omega}) + \sigma_t(\boldsymbol{x})u(\boldsymbol{x}, \boldsymbol{\omega}) = \sigma_s(\boldsymbol{x})(Su)(\boldsymbol{x}, \boldsymbol{\omega}) + f(\boldsymbol{x}, \boldsymbol{\omega}), \quad \boldsymbol{x} \in D, \boldsymbol{\omega} \in S^2.$$
 (5.5)

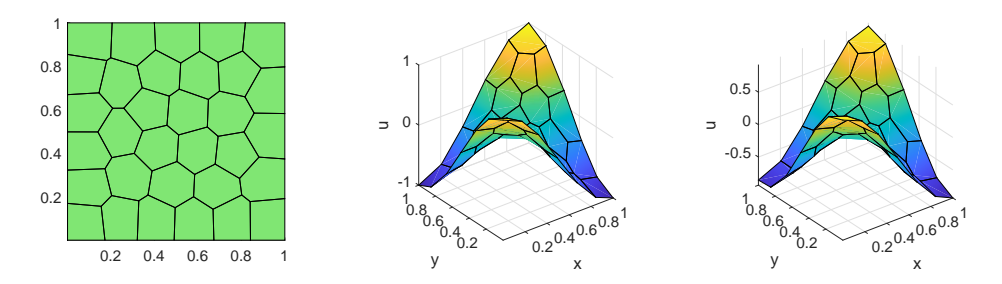


Fig. 4: Exact and numerical solutions for linear virtual element method

Here, D is a domain in \mathbb{R}^3 and S^2 denotes the unit sphere in \mathbb{R}^3 , $u(\boldsymbol{x}, \boldsymbol{\omega})$ is a function of three space variables \boldsymbol{x} and two angular variables $\boldsymbol{\omega}$. We impose an inflow boundary value condition

$$u(\boldsymbol{x}, \boldsymbol{\omega}) = \alpha(\boldsymbol{x}, \boldsymbol{\omega}), \quad (\boldsymbol{x}, \boldsymbol{\omega}) \in \Gamma_{-},$$

where Γ_{-} is defined by

$$\Gamma_{-} = \{ (\boldsymbol{x}, \boldsymbol{\omega}) : \boldsymbol{x} \in \partial D, \ \boldsymbol{\omega} \in S^2, \quad \boldsymbol{n}(\boldsymbol{x}) \cdot \boldsymbol{\omega} < 0 \}.$$

The symbol S on the right-hand side of (5.5) is defined by

$$(Su)(\boldsymbol{x}, \boldsymbol{\omega}) = \int_{S^2} g(\boldsymbol{x}, \boldsymbol{\omega} \cdot \hat{\boldsymbol{\omega}}) u(\boldsymbol{x}, \hat{\boldsymbol{\omega}}) d\sigma(\hat{\boldsymbol{\omega}})$$

with g being a nonnegative normalized phase function

$$\int_{S^2} g(\boldsymbol{x}, \boldsymbol{\omega} \cdot \hat{\boldsymbol{\omega}}) d\sigma(\hat{\boldsymbol{\omega}}) = 1, \quad \boldsymbol{x} \in D, \boldsymbol{\omega} \in S^2.$$

In most applications, the function g is assumed to be independent of x. One well-known example considered in this paper is the Henyey-Greenstein phase function

$$g(t) = \frac{1 - \eta^2}{4\pi (1 + \eta^2 - 2\eta t)^{3/2}}, \quad t \in [-1, 1],$$

where the parameter $\eta \in (-1,1)$ measures the strength of forward peakedness of the phase function.

For this problem, we consider the discretization by using the sparse grid discrete ordinate discontinuous Galerkin method proposed in [25]. As shown in the section for numerical tests there, the final linear system can be written as $D\hat{U} = F$, with the matrices written in the following block form:

$$m{D} = \left[egin{array}{c} m{D}^{(1)} \ dots \ m{D}^{(L)} \end{array}
ight], \quad \hat{m{U}} = \left[egin{array}{c} \hat{m{U}}^1 \ dots \ \hat{m{U}}^L \end{array}
ight], \quad m{F} = \left[egin{array}{c} m{F}^{(1)} \ dots \ m{F}^{(L)} \end{array}
ight].$$

This linear system is too large for the implementation of the Schrödingerization-form approach on a classical computer. Therefore, we solve it using the block Gauss-Seidel iteration method, with the Schrödingerization form applied to the linear systems encountered in each iteration.

Example 5.5. We take $\sigma_t = 2$, $\sigma_s = 1$ and $\eta = 0$. With the right-side hand function

$$f(\mathbf{x}, \boldsymbol{\omega}) = \pi s_1 \cos(\pi x_1) \sin(\pi x_2) \sin(\pi x_3) + \pi s_2 \sin(\pi x_1) \cos(\pi x_2) \sin(\pi x_3) + \pi s_3 \sin(\pi x_1) \sin(\pi x_2) \cos(\pi x_3) + \sin(\pi x_1) \sin(\pi x_2) \sin(\pi x_3),$$

where $\omega = (s_1, s_2, s_3)$, the exact solution is

$$u(\boldsymbol{x}, \boldsymbol{\omega}) = \sin(\pi x_1) \sin(\pi x_2) \sin(\pi x_3).$$

Here we consider the first example from [25] with the same discretization parameters. Since the linear systems encountered in each Gauss-Seidel iteration remain large in size, for simplicity, we diagonalize the equation (3.2) and solve it exactly. The exact and numerical solutions, displayed in Fig. 5, exhibit good agreement.

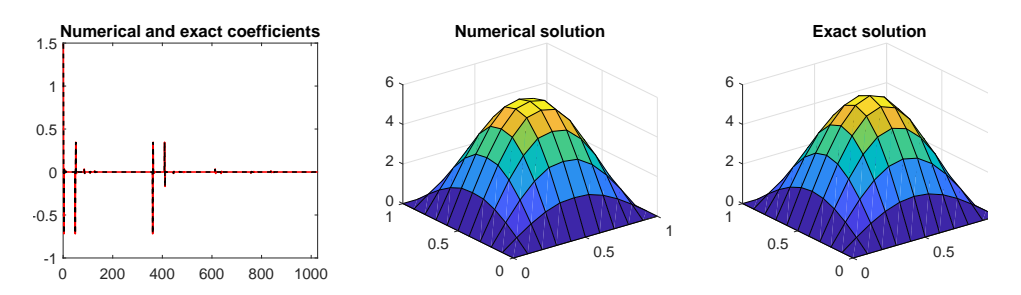


Fig. 5: Exact and numerical solutions for the radiative transfer equation

6 Improved dependence on condition number by preconditioning

As indicated in Remark 4.2, the time complexity of our algorithm has a quadratic dependence on the condition number. In this section, we develop a quantum preconditioning algorithm that employs the well-known BPX multilevel preconditioner for the finite element discretization of the two-dimensional Poisson equation in Section 5.2. For simplicity, we assume that both B and A are symmetric positive definite.

Since B and BA are not sparse in general, we need to consider the block-encoding input model as was done in [18,19]. Let Ω be a polygonal domain with \mathcal{T}_0 being an initial triangulation of Ω . By connecting the midpoints of the edges of each triangle, we can obtain a refined mesh \mathcal{T}_1 . Continuing in this manner, we obtain a sequence of nested meshes $\mathcal{T}_0, \mathcal{T}_1, \dots, \mathcal{T}_J$. For each mesh \mathcal{T}_j , we define V_j as the continuous piecewise linear finite element space, as in (5.2), with \mathcal{T}_h replaced by \mathcal{T}_j . This procedure generates a nested sequence of subspaces of V_J : $V_0 \subset V_1 \subset \dots \subset V_J$. Let $V_h = V_J$. The corresponding linear algebraic system is given in (5.3). Let $\{\varphi_{j,i}\}_{i=1}^{N_j}$ be the nodal basis of V_j . The matrix $I_j \in \mathbb{R}^{N \times N_j}$ represents the nodal basis of V_j in terms of the nodal basis of V_h , i.e.,

$$(\varphi_{j,1}, \varphi_{j,2}, \cdots, \varphi_{j,N_j}) = (\varphi_1, \varphi_2, \cdots, \varphi_N)I_j.$$

According to the discussion in [19, 26], the BPX preconditioner for the stiffness matrix A can be written as

$$B = \sum_{j=0}^{J} S_j S_j^T, \qquad S_j = h_j^{(2-d)/2} I_j, \tag{6.1}$$

where h_j is the mesh size of \mathcal{T}_j . Let I_i^{i+1} be the prolongation matrix from \mathcal{T}_i to \mathcal{T}_{i+1} . Then, we have $I_j = I_{J-1}^J I_{J-2}^{J-1} \cdots I_{j+1}^{j+2} I_j^{j+1}$. This formulation enables the use of the LCU technique to linearly combine the block encodings of these substructures. The block encoding of each substructure can

be obtained from the corresponding sparse query model. For further details, we refer the reader to Section 5.3 in [19] for the block encoding of prolongation matrices. It is worth noting that the block encoding of B is simpler than that of $S = [S_0, S_1, \dots, S_J]$ used in [19], where a generalized block encoding is required.

We continue with Example 5.3. In this case, we consider the kernel function $e^{-|p|}$ although it does not provide optimal error estimate in the p-direction. We begin by considering the \mathbb{P}_1 -Lagrange element. The initial mesh is shown in Fig. 2a. The computational domain for p is now truncated as [-L, R], given by

$$R = \mathcal{O} \left(\kappa^- \log \frac{\kappa(W)}{\varepsilon} + \log \frac{1}{\varepsilon} + \frac{1}{2} \right), \quad L = \mathcal{O} \left(\kappa^+ \log \frac{\kappa(W)}{\varepsilon} + \log \frac{1}{\varepsilon} + \frac{1}{2} \right),$$

where

$$\kappa^{\pm} = \frac{\lambda_{\max}^{\pm}(BA + AB)}{2\lambda_{\min}(BA)},$$

with $\lambda_{\text{max}}^+(C)$ and $\lambda_{\text{max}}^-(C)$ denoting the maximum positive and negative eigenvalues of C in absolute value, respectively. We take $N_p = 2^{11}$ for the discrete Fourier transform. We select an evolution time T = 15, which is sufficient to achieve satisfactory performance. The results for the first three meshes are the same in Fig. 2. Additionally, the convergence rates in the L^2 and H^1 norms are shown in Fig. 6. It is evident that the errors in both the L^2 and H^1 norms exhibit second-order and first-order convergence, respectively, which aligns with the standard theoretical predictions in FEMs.

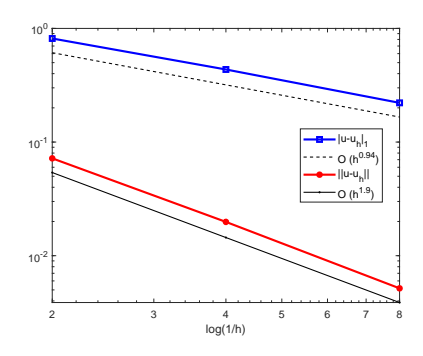


Fig. 6: Convergence rates for \mathbb{P}_1 -Lagrange elements for the preconditioned system

For the \mathbb{P}_2 -Lagrange elements, the multilevel methods still use linear finite elements as the coarse spaces. This results in the following nested finite element spaces: $V_0 \subset V_1 \subset \cdots \subset V_J \subset V_h$, where V_0, \cdots, V_J correspond to \mathbb{P}_1 -Lagrange elements, and V_h represents the space for higher-order elements. It is important to note that both V_J and V_h correspond to the finest mesh. We only need to include the transfer between linear and higher-order elements on the same grid \mathcal{T}_J . We continue with Example 5.3, using the same setup for the \mathbb{P}_1 -elements. The exact and numerical solutions for the second mesh are shown in Fig. 7, where the results remain satisfactory. However, due to the loss of precision in the p-direction, the theoretical convergence rates for the FEMs, as shown in Fig. 8, are not achieved.

For the S given in (6.1), let us check the recover range of p for the algorithm in [19] for the \mathbb{P}_1 Lagrange elements. We present the errors for different values of p when recovering the solution in

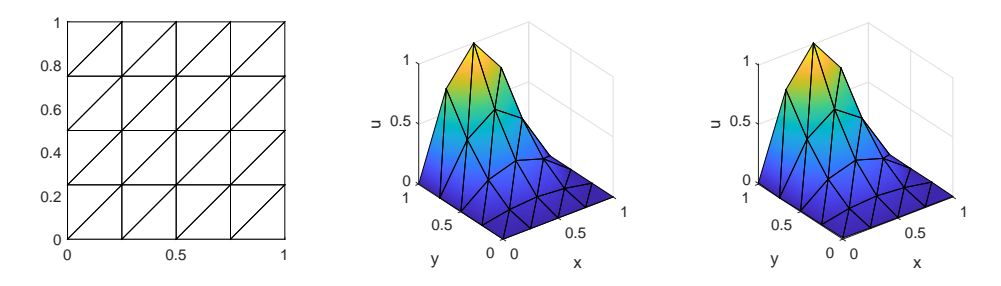


Fig. 7: Exact and numerical solutions for \mathbb{P}_2 -Lagrange elements

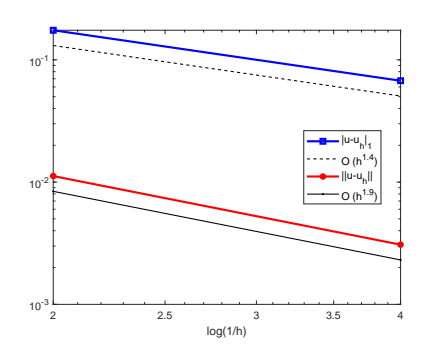


Fig. 8: Convergence rates for \mathbb{P}_2 -Lagrange elements

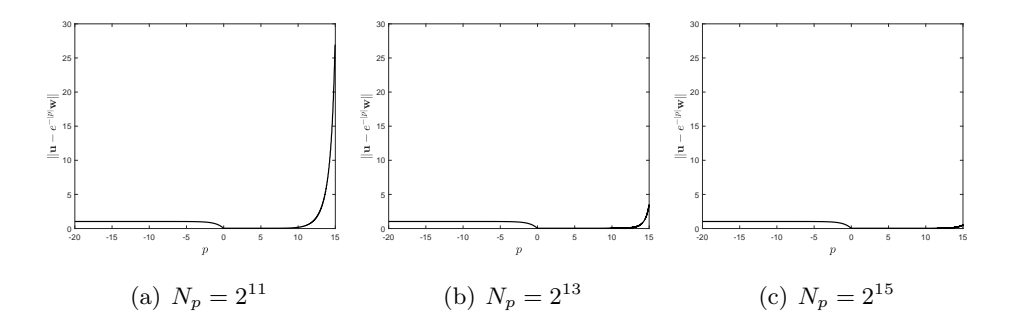


Fig. 9: Errors of $\|\boldsymbol{u} - e^{|p|}\boldsymbol{w}\|$ for different values of p (see [19])

Fig. 9a for the first mesh. It is evident that the solution can be recovered theoretically for $p \ge 1/2$. However, when p is relatively large, the accuracy may degrade, as shown in Fig. 9. This implies that considering the steady-state solution to the ODEs for the non-symmetric preconditioning system BAx = Bb, as mentioned in the introduction, is not appropriate. This reinforces the advantage of our algorithm in this regard, as the algorithm in [19] may need to recover the solution for $p \ge T \log(1/\varepsilon)$, which can become large when T is large.

CRediT authorship contribution statement

The authors are listed in alphabetical order. All authors contributed equally to this work.

Acknowledgements

Y Yang is supported by the National Natural Science Foundation of China Project (No. 12261131501), National Foreign Experts Program (No.S20240066), the Project of Scientific Research Fund of the Hunan Provincial Science and Technology Department (No.2023GK2029, No.2024 JC1003, No.2024JJ1008), and "Algorithmic Research on Mathematical Common Fundamentals" Program for Science and Technology Innovative Research Team in Higher Educational Institutions of Hunan Province of China. Y Yu is supported by the National Science Foundation for Young Scientists of China (No. 12301561) and the Key Project of Scientific Research Project of Hunan Provincial Department of Education (No. 24A0100), with additional partial support from NSFC grant No. 12341104.

References

- [1] D. An, A. M. Childs, and L. Lin. Quantum algorithm for linear non-unitary dynamics with near-optimal dependence on all parameters. arXiv:2312.03916, 2023.
- [2] S. Jin, N. Liu, and Y. Yu. Quantum simulation of partial differential equations via Schrödingerisation. *Phys. Rev. Lett.*, 133:230602, 2024.
- [3] S. Jin, N. Liu, and Y. Yu. Quantum simulation of partial differential equations: Applications and detailed analysis. *Phys. Rev. A*, 108:032603, 2023.
- [4] A. M. Childs, R. Kothari, and R. D. Somma. Quantum algorithm for systems of linear equations with exponentially improved dependence on precision. SIAM J. Comput., 46(6):1920–1950, 2017.
- [5] M. A. Nielsen and I. L. Chuang. Quantum Computation and Quantum Information. Cambridge, New York, 2010.
- [6] R. J. Lipton and K. W. Regan. Quantum Algorithm via Linear Algebra. Cambridge, Massachusetts, 2010.
- [7] D. Deutsch and R. Jozsa. Rapid solution of problems by quantum computation. *Proc. R. Soc. London, Ser. A*, 439:553, 1992.
- [8] P. W. Shor. Polynomial-time algorithms for prime factorization and discrete logarithms on a quantum computer. SIAM J. Comput., 26:1484, 1997.
- [9] A. W. Harrow, A. Hassidim, and S. Lloyd. Quantum algorithm for linear systems of equations. *Phys. Rev. Lett.*, 103(15):150502, 4 pp., 2009.
- [10] P. C. S. Costa, D. An, Y. R. Sanders, Y. Su, R. Babbush, and D. W. Berry. Optimal scaling quantum linear-systems solver via discrete adiabatic theorem. *PRX quantum*, 3(4):040303, 2022.
- [11] A. Ambainis. Variable time amplitude amplification and quantum algorithms for linear algebra problems. *LIPIcs. Leibniz Int. Proc. Inform.*, 14:636–647, 2012.
- [12] D. An and L. Lin. Quantum linear system solver based on time-optimal adiabatic quantum computing and quantum approximate optimization algorithm. ACM Trans. Quantum Comput., 3(2):1–28, 2022.
- [13] L. Lin and Y. Tong. Optimal polynomial based quantum eigenstate filtering with application to solving quantum linear systems. *Quantum Inf. Process.*, 4:361, 2020.
- [14] A. Dranov, J. Kellendonk, and R. Seiler. Discrete time adiabatic theorems for quantum mechanical systems. J. Math. Phys., 39:1340, 1998.
- [15] Y. Subasi and R. D. Somma. Quantum algorithms for systems of linear equations inspired by adiabatic quantum computing. Phys. Rev. Lett., 122:060504, 2019.

- [16] J Hu, S. Jin, and L. Zhang. Quantum algorithms for multiscale partial differential equations. Multiscale Model. Simul., 22(3):1030–1067, 2024.
- [17] S. Jin and N. Liu. Analog quantum simulation of partial differential equations. *Quantum Sci. Technol.*, 9(3):035047, 2024.
- [18] M. Deiml and D. Peterseim. Quantum realization of the finite element method. $arXiv:2403.19512,\ 2024.$
- [19] S. Jin, N. Liu, C. Ma, and Y. Yu. Quantum preconditioning method for linear systems problems via Schrödingerization. *Preprint*, 2024.
- [20] D. An, J. Liu, and L. Lin. Linear combination of Hamiltonian simulation for non-unitary dynamics with optimal state preparation cost. *Phys. Rev. Lett.*, 131(15):150603, 2023.
- [21] J. S. Hesthaven, S. Gottlieb, and D. Gottlieb. *Spectral Methods for Time-dependent Problems*. Cambridge University Press, 2007.
- [22] D. Kahaner, C. Moler, and S. Nash. Numerical Methods and Software. Prentice Hall, 1989.
- [23] S. C. Brenner and L. R. Scott. The Mathematical Theory of Finite Element Methods. Springer, New York, 2008.
- [24] L. Beirão Da Veiga, F. Brezzi, and L. D. Marini. Virtual elements for linear elasticity problems. SIAM J. Numer. Anal., 51(2):794–812, 2013.
- [25] J. G. Huang and Y. Yu. A sparse grid discrete ordinate discontinuous Galerkin method for the radiative transfer equation. *Commun. Comput. Phys.*, 30(4):1009–1036, 2021.
- [26] J. Xu. Iterative methods by space decomposition and subspace correction. SIAM Rev., (4):581–613, 1992.